The Astrophysical Journal, 770:47 (7pp), 2013 June 10 doi:10.1088/0004-637X/770/1/47

CONSTRAINING PRIMORDIAL MAGNETIC FIELDS THROUGH LARGE-SCALE STRUCTURE

Tina Kahniashvili[1,2,3], Yurii Maravin[4], Aravind Natarajan[1], Nicholas Battaglia[1], and Alexander G. Tevzadze[5]
[1] McWilliams Center for Cosmology and Department of Physics, Carnegie Mellon University, 5000 Forbes Avenue, Pittsburgh, PA 15213, USA; tinatin@andrew.cmu.edu
[2] Department of Physics, Laurentian University, Ramsey Lake Road, Sudbury, ON P3E 2C, Canada
[3] Abastumani Astrophysical Observatory, Ilia State University, 3-5 Cholokashvili Avenue, Tbilisi 0194, Georgia
[4] Department of Physics, Kansas State University, 116 Cardwell Hall, Manhattan, KS 66506, USA
[5] Faculty of Exact and Natural Sciences, Javakhishvili Tbilisi State University, 3 Chavchavadze Avenue, Tbilisi 0128, Georgia
Received 2012 November 17; accepted 2013 April 15; published 2013 May 22

ABSTRACT

We study primordial magnetic field effects on the matter perturbations in the universe. We assume magnetic field generation prior to the big bang nucleosynthesis (BBN), i.e., during the radiation-dominated epoch of the universe expansion, but do not limit analysis by considering a particular magnetogenesis scenario. Contrary to previous studies, we limit the total magnetic field energy density and not the smoothed amplitude of the magnetic field at large (of the order of 1 Mpc) scales. We review several cosmological signatures, such as halo abundance, thermal Sunyaev–Zel'dovich effect, and Lyα data. For a cross-check, we compare our limits with that obtained through the cosmic microwave background faraday rotation effect and BBN. The limits range between 1.5 nG and 4.5 nG for $n_B \in (-3; -1.5)$.

Key words: large-scale structure of universe – primordial nucleosynthesis

Online-only material: color figures

1. INTRODUCTION

Observations show that galaxies have magnetic fields with a component that is coherent over a large fraction of the galaxy with a field strength of the order of 10^{-6} G (Beck et al. 1996; Widrow 2002; Vallee 2004). These fields are supposed to be the result of amplification of initial weak seed fields of an unknown nature. A recent study, based on the correlation of Faraday rotation measures and Mg II absorption lines (which trace halos of galaxies), indicates that coherent μG-strength magnetic fields were already in place in normal galaxies (like the Milky Way) when the universe was less than half its present age (Kronberg et al. 2008). This places strong constraints both on the strength of the initial magnetic seed field and the timescale required for amplification. Understanding the origin and evolution of these fields is one of the challenging questions of modern astrophysics. There are two generation scenarios currently under discussion: a bottom-up (astrophysical) one, where the necessary seed field is generated on smaller scales, and a top-down (cosmological) scenario, where the seed field is generated prior to galaxy formation in the early universe on scales that are large now. More precisely, the astrophysical seed field sources include battery mechanisms, plasma processes, or a simple transport of magnetic flux from compact systems (e.g., stars, active galactic nuclei), where magnetic field generation can be extremely fast because of the rapid rotation (Kulsrud & Zweibel 2008). Obviously, the correlation length of such a seed field cannot be larger than a characteristic galactic length scale, and is typically much smaller. In the cosmological seed field scenario (Kandus et al. 2011), the seed field correlation length could be significantly larger than the current Hubble radius if it were generated by quantum fluctuations during inflation. There are different options for seed field amplification, ranging from the MHD dynamo to the adiabatic compression of the magnetic field lines during structure formation (Beck et al. 1996). The presence of turbulence in cosmic plasma plays a crucial role in both of these processes. The MHD turbulence was investigated a long time ago when considering the processes in astrophysical plasma, while there is a lack of studies when addressing the turbulence effects in cosmological contexts (Biskamp 2003). In the late stages of evolution, the energy density present in the form of turbulent motions in clusters can be as large as 5%–10% of the thermal energy density (Kravtsov & Borgani 2012). This can influence the physics of clusters (Subramanian et al. 2006) and/or at least should be modeled correctly when performing large-scale simulations (Vazza et al. 2006; Feng et al. 2009). The proper accounting of the MHD turbulence effects is still under discussion (Springel 2010). Both astrophysical and primordial turbulence might have distinctive observational signatures. As we have already noted above, the most direct signature of MHD turbulence is the observed magnetic fields in clusters and galaxies.

Galactic magnetic fields are usually measured through the induced Faraday rotation effect (see Vallee 2004) and, as mentioned above, the coherent field magnitude is of the order of a few μG with a typical coherence scale of 10 kpc.[6] On larger scales, there have been recent claims of an observed lower limit of the order of 10^{-15}–10^{-16} G on the intergalactic magnetic field (Neronov & Vovk 2010; Tavecchio et al. 2010; Dolag et al. 2011), assuming a correlation length of $\lambda \geqslant 1$ Mpc, or possibly two orders of magnitude smaller (Dermer et al. 2011). An alternative approach to explain the blazar spectra anomalies has been discussed by Broderick et al. (2012), where two-beam plasma instabilities were considered.[7] Although these instabilities are well tested through numerical experiments for laboratory plasma for a given set of parameters such as temperature and energy densities of beams and background, its efficiency might be questioned for cosmological plasma because of a significantly different (several orders of magnitudes) beam

[6] On the other hand, simulations starting from constant comoving magnetic fields of 10^{-11}G show cluster-generating fields sufficiently large to explain Faraday rotation measurements (Dolag et al. 2002; Banerjee & Jedamzik 2003).
[7] The recent study (Arlen et al. 2012) claims that proper accounting for uncertainties of the source modeling leads to consistence with a zero magnetic field hypothesis.

and background temperature and energy densities. Prior to these observations, the intergalactic magnetic field was limited only to be smaller than a few nG from cosmological observations, such as the limits on the cosmic microwave background (CMB) radiation polarization plane rotation (Yamazaki et al. 2010) and on the Faraday rotation of polarized emission from distant blazars and quasars (Blazi et al. 1999).

In the present paper, we consider the presence of a primordial magnetic field in the universe and give a simplified description of its effect on large-scale structure formation. We assume that the magnetic field has been generated during the radiation-dominated epoch and prior to big bang nucleosynthesis (BBN). Since the magnetic energy density contributes to the relativistic component, the presence of such a magnetic field affects the moment of matter-radiation equality, shifting it to later stages. We focus on the linear matter power spectrum in order to show that even if the total energy density present in the magnetic field (and, as a consequence, in magnetized turbulence) is small enough, its effects might be substantial, and the effect becomes stronger due to nonlinearity of processes under consideration.

It has become conventional to derive the cosmological effects of a seed magnetic field by using its spectral shape (parameterized by the spectral index n_B) and the smoothed value of the magnetic field (B_λ) at a given scale λ (which is usually taken to be 1 Mpc). In Kahniashvili et al. (2011), we developed a different and more adequate formalism based on the effective magnetic field value that is determined by the total energy density of the magnetic field. Such an approach has been mostly motivated by the simplest energy constraint on the magnetic field generated in the early universe. In order to preserve BBN physics, only 10% of the relativistic energy density can be added to the radiation energy density, leading to the limit on the total magnetic field energy density corresponding to the effective magnetic field value of the order of 10^{-6} G. More precise studies of the influence of the primordial magnetic field on the expansion rate and the abundance of light elements performed recently (Yamazaki & Kusakabe 2012; Kawasaki & Kusakabe 2012) lead to effective magnetic field amplitudes of the order of $1.5\text{–}1.9 \times 10^{-6}$ G.

The described formalism has been applied to describe two different effects of the primordial magnetic field: the CMB Faraday rotation effect and mass dispersion (Kahniashvili et al. 2010). As a striking consequence, we show that even an extremely small smoothed magnetic field of 10^{-29} G at 1 Mpc, with the Batchelor spectral shape ($n_B = 2$) at large scales, can leave detectable signatures in CMB or Large Scale Structure (LSS) statistics. In the present investigation we focus on the thermal Sunyaev–Zel'dovich (tSZ) effect, the cluster number density, and Lyα data. The large-scale-based tests, such as tSZ, Lyα, cosmic shear (gravitational lensing), and X-ray cluster surveys, have been studied in Shaw & Lewis (2012), Tashiro & Sugiyama (2011), Tashiro et al. (2012), Fedeli & Moscardini (2012), and Pandey & Sethi (2013), but again in the context of a smoothed magnetic field. Another possible observational signature of large-scale correlated cosmological magnetic fields may be found in cosmic-ray acceleration and corresponding gamma ray signals (see Essey et al. 2012 and references therein). These observational signatures of the primordial magnetic field are beyond the scope of the present paper. We also perform a more precise data analysis, and we do not focus only on inflation-generated magnetic fields.

The paper is organized as follows. In Section 2, we briefly review the effective magnetic field formalism and discuss the effect on the density perturbations. In Section 3, we review observational consequences and derive the limits on primordial magnetic fields. The conclusions are given in Section 4.

2. MODELING THE MAGNETIC-FIELD-INDUCED MATTER POWER SPECTRUM

We assume that the primordial magnetic field has been generated during or prior to BBN, i.e., well during the radiation-dominated epoch.[8] A stochastic Gaussian magnetic field is fully described by its two-point correlation function. For simplicity, we consider the case of a non-helical magnetic field[9] for which the two-point correlation function in wavenumber space is (Kahniashvili et al. 2010)

$$\langle B_i^*(\mathbf{k}) B_j(\mathbf{k}')\rangle = (2\pi)^3 \delta^{(3)}(\mathbf{k}-\mathbf{k}') P_{ij}(\hat{\mathbf{k}}) P_B(k). \quad (1)$$

Here i and j are spatial indices; $i, j \in (1, 2, 3)$, $\hat{k}_i = k_i/k$ is a unit wavevector, $P_{ij}(\hat{\mathbf{k}}) = \delta_{ij} - \hat{k}_i \hat{k}_j$ is the transverse plane projector, $\delta^{(3)}(\mathbf{k}-\mathbf{k}')$ is the Dirac delta function, and $P_B(k)$ is the power spectrum of the magnetic field.

The smoothed magnetic field B_λ is defined through the mean-square magnetic field, ${B_\lambda}^2 = \langle \mathbf{B}(\mathbf{x}) \cdot \mathbf{B}(\mathbf{x})\rangle|_\lambda$, where the smoothing is done on a comoving length λ with a Gaussian smoothing kernel function $\propto \exp[-x^2/\lambda^2]$. Corresponding to the smoothing length λ is the smoothing wavenumber $k_\lambda = 2\pi/\lambda$. The power spectrum $P_B(k)$ is assumed to depend on k as a simple power-law function on large scales, $k < k_D$ (where k_D is the cutoff wavenumber),

$$P_B(k) = P_{B0} k^{n_B} = \frac{2\pi^2 \lambda^3 B_\lambda^2}{\Gamma(n_B/2+3/2)} (\lambda k)^{n_B}, \quad (2)$$

and assumed to vanish on small scales where $k > k_D$.

We define the effective magnetic field $B_{\rm eff}$ through the magnetic energy density $\rho_B = B_{\rm eff}^2/(8\pi)$. In terms of the smoothed field, the magnetic energy density is given by

$$\rho_B(\eta_0) = \frac{B_\lambda^2 (k_D \lambda)^{n_B+3}}{8\pi \Gamma(n_B/2+5/2)}, \quad (3)$$

and thus $B_{\rm eff} = B_\lambda (k_D\lambda)^{(n_B+3)/2}/\sqrt{\Gamma(n_B/2+5/2)}$. For the scale-invariant spectrum, $n_B = -3$ and $B_{\rm eff} = B_\lambda$ for all values of λ. The scale-invariant spectrum is the only case where the values of the effective and smoothed fields coincide. For causal magnetic fields with $n_B = 2$ (Durrer & Caprini 2003), the smoothed magnetic field value is extremely small for moderate values of the magnetic field.

We also need to determine the cutoff scale k_D. We assume that the cutoff scale is determined by the Alfvén wave damping scale $k_D \sim v_A L_S$, where v_A is the Alfvén velocity and L_S is the Silk damping scale (Jedamzik et al. 1998; Subramanian & Barrow 1998). Such a description is more appropriate when dealing with

[8] Note that some results of this paper can also be applied to the case when magnetic fields are generated during the matter-dominated epoch, but with several "caveats": in this case the BBN limits will not be valid since the magnetic field will not be present during matter-radiation equality and will not affect the expansion rate of the early universe and light element abundances. On the other hand, if the magnetic field has been generated prior to recombination, the CMB limits must be used. For any other field generated before reionization and first structure formation, only the large-scale structure tests may apply. We thank the anonymous referee for pointing out this issue.

[9] We limit ourselves to considering a non-helical magnetic field because the density perturbations, and as a result the matter power spectrum, are not affected by the presence of magnetic helicity.

a homogeneous magnetic field, and the Alfvén waves are the fluctuations of $\mathbf{B}_1(\mathbf{x})$ with respect to a background homogeneous magnetic field $\mathbf{B}_0$ ($|\mathbf{B}_1| \ll |\mathbf{B_0}|$). In the case of a stochastic magnetic field, we generalize the Alfvén velocity definition from Mack et al. (2002) by referring to the analogy between the effective magnetic field and the homogeneous magnetic field. Assuming that the Alfvén velocity is determined by $B_{\rm eff}$, a simple computation gives the expression of k_D in terms of $B_{\rm eff}$:

$$\frac{k_D}{1\,{\rm Mpc}^{-1}} = 1.4\sqrt{\frac{(2\pi)^{n_B+3}h}{\Gamma(n_B/2+5/2)}}\left(\frac{10^{-7}{\rm G}}{B_{\rm eff}}\right). \quad (4)$$

Here h is the Hubble constant in units of 100 km s^{-1} Mpc^{-1}.

Note that any primordial magnetic field generated prior or during BBN should satisfy the BBN bound (for recent studies of primordial magnetic field effects on BBN processes and corresponding limits, see Yamazaki & Kusakabe 2012; Kawasaki & Kusakabe 2012). Assuming that the magnetic field energy density is not damped away by MHD processes, the BBN limit on the effective magnetic field strength $B_{\rm eff} \leqslant 1.5$–$1.9 \times 10^{-6}$ G, while transferred in terms of B_λ the BBN bounds result in extremely small values for causal fields; see Caprini & Durrer (2001) and Kahniashvili et al. (2011).

The primordial magnetic field affects all three kinds of metric perturbations: scalar (density), vector (vorticity), and tensor (gravitational waves) modes through the Einstein equations. The primordial magnetic field generates a matter perturbation power spectrum with a different shape compared to the standard ΛCDM model. As we noted above in this paper, we focus on matter perturbations. As has been shown by Kim et al. (1996) and Gopal & Sethi (2005), the magnetic-field-induced matter power spectrum $P(k) \propto k^4$ for $n_B > -1.5$ and $\propto k^{2n_B+7}$ for $n_B \leqslant -1.5$. This in turn affects the formation of rare objects like galaxy clusters that sample the exponential tail of the mass function. Shaw & Lewis (2012) study the formation of the magnetic field matter power spectrum through analytical description in great detail and provide a modified version of CAMB that includes the possibility of a non-zero magnetic field. We have used the CAMB code to determine the matter power spectra for a wide range of the magnetic field amplitudes and spectral indices. These spectra are shown in Figure 1. It is obvious that the matter power spectrum is sensitive to the values of the cosmological parameters: the Hubble constant in units of 100 km s^{-1} Mpc^{-1}, h, Ω_M, and Ω_b, as well as the density parameter of each dark matter component, i.e., $\Omega_{\rm cdm}$ and Ω_ν (here M, b, cdm, and ν indices refer to matter, baryons, cold dark matter, and neutrinos, respectively, and Ω is the density parameter). To generate the matter plot we assume the standard flat ΛCDM model with zero curvature and use the following cosmological parameters: $\Omega_b h^2 = 0.022$, $\Omega_C h^2 = 0.1125$, and $h = 0.71$. For simplicity, we assume massless neutrinos with three generations.[10] As we can see, the increase of the smoothed field amplitude results in the additional power spectrum shift to the left, while increasing the value of n_B makes the vertical shift. As we can see, the large-scale tail (small wavenumbers) of the matter power spectrum is unaffected by the presence of the magnetic field. Below we address some of effects induced by the presence of the magnetic field, especially on large scales.

[10] The standard ΛCDM model matter power spectrum $P_{\Lambda{\rm CDM}}(k)$ assumes a close to scale-invariant (Harrison-Peebles-Yu-Zel'dovich) post-inflation energy density perturbation power spectrum $P_0(k) \propto k^n$, with $n \sim 1$.

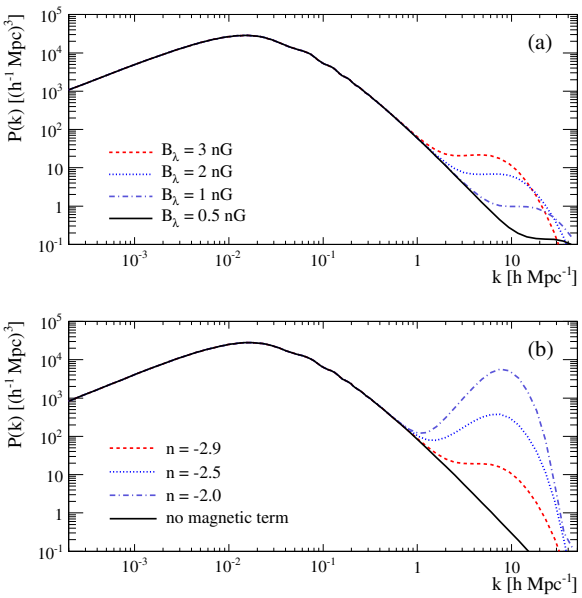

Figure 1. Magnetic field matter power spectra for $n_B = -2.9$ with different values of B_λ (a) and for $B_\lambda = 3$ nG with different values of n_B (b).
(A color version of this figure is available in the online journal.)

3. OBSERVATIONAL SIGNATURES

Primordial magnetic fields can play a potentially important role in the formation of the first large-scale structures.

3.1. The Thermal Sunyaev–Zel'dovich Effect

As demonstrated in Shaw & Lewis (2012), Tashiro & Sugiyama (2011), and Paoletti & Finelli (2012), the strength of the primordial magnetic field affects the growth of structure. The power spectrum of secondary anisotropies in the CMB caused by the thermal tSZ effect is a highly sensitive probe of the growth of structure (e.g., Komatsu & Seljak 2002). The tSZ angular power spectrum probes the distribution of galaxy clusters on the sky essentially out to any redshift. At $l \simeq 3000$, half of the contribution to the SZ power spectrum comes from matter halos with masses greater than $\sim 2 \times 10^{14}\,M_\odot$ at redshifts less than $z \simeq 0.5$; see Battaglia et al. (2012) and Trac et al. (2011).

All the previous work on how primordial magnetic fields affect the tSZ power spectrum have used the model from Komatsu & Seljak (2002), here referred to as the KS model, which has been shown to be incompatible with recent observations of clusters (Arnaud et al. 2010) and tSZ power spectrum measurements by Lueker et al. (2009). Using the KS model for primordial magnetic field studies also ignores all the recent advancements in tSZ power spectrum theory and predictions that illustrate the importance of properly modeling the detailed astrophysics of the intracluster medium (e.g., Battaglia et al. 2010, 2012; Shaw et al. 2010; Trac et al. 2011). We modify the code described in Shaw & Lewis (2012) to include these improvements by changing the pressure profile used in their model from KS to the profile given in Battaglia et al. (2010, 2012). The results obtained using the modified pressure profile are shown in Figure 2 with the greatest difference being the amplitude of the new tSZ power spectrum is approximately two times lower than previous predictions and below the current observational constraint from Actama Cosmology Telescope (ACT; Dunkley et al. 2011) and South Pole Telescope (SPT; Reichardt et al. 2012) at $\ell = 3000$. Updating the theory predictions for the tSZ

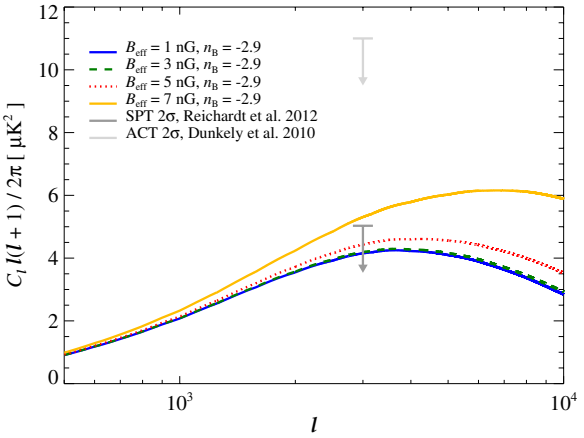

Figure 2. tSZ power spectrum predictions at 150 GHz varying the primordial magnetic field model at fixed cosmological parameters, most importantly $\sigma_8 = 0.8$. These predictions are compared against the recent upper limits from ACT (Dunkley et al. 2011) and SPT (Reichardt et al. 2012) at $\ell = 3000$. The current upper limits on the tSZ amplitude at $\ell = 3000$ do not constrain the primordial magnetic field parameters $B_{\rm eff}$ and n_B as well as other observations.
(A color version of this figure is available in the online journal.)

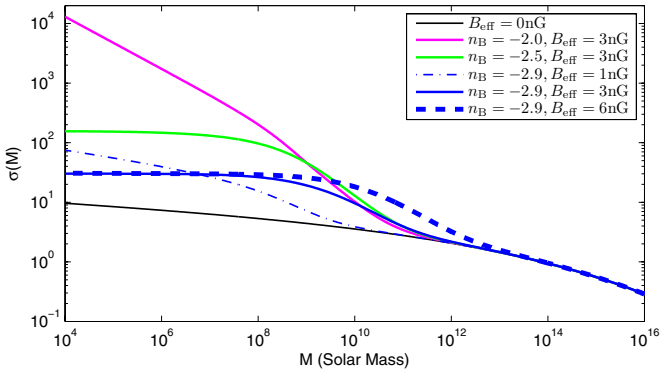

Figure 3. $\sigma(M, z = 0)$ for different effective magnetic field values $B_{\rm eff}$ and spectral index n_B.
(A color version of this figure is available in the online journal.)

power significantly reduces the constraints put on primordial magnetic field parameters using these observations. In Figure 2, we illustrate that magnetic fields with an effective amplitude of order 5 nG are almost excluded. Given that there is additional uncertainty in the theoretical modeling of the tSZ (e.g., Battaglia et al. 2010, 2012; Shaw et al. 2010; Trac et al. 2011), combined with significant contributions from other secondary sources (Reichardt et al. 2012; Dunkley et al. 2011) around $\ell \sim 3000$, for example, from dusty star-forming galaxies, future tSZ power spectrum measurements are not going to be competitive in constraining primordial magnetic field parameters.

3.2. Halo Number Density

The predicted halo number density $N_{\rm pred}(M > M_0, z)$ depends on the considered cosmological model. One of the important characteristics of a cosmological model is the linear matter power spectrum that we reviewed in Section 2 above. Below we discuss the halo number count dependence on the presence of the magnetic field.

The halo mass function at a redshift z is $N(M > M_0, z) = \int_{M_0}^{\infty} dM n(M, z)$, where $n(M, z)dM$ is the comoving number density of collapsed objects with mass lying in the interval $(M, M + dM)$, and it can be expressed as

$$n(M, z) = \frac{2\rho_M}{M} \nu f(\nu) \frac{d\nu}{dM}. \quad (5)$$

The multiplicity function $\nu f(\nu)$ is a universal function of the peak height (Press & Schechter 1974) $\nu = \delta_C/\sigma(R)$, where $\sigma(R, z)$ is the rms amplitude of density fluctuations smoothed over a sphere of radius $R = (3M/4\pi\rho_M)^{1/3}$, and the critical density contrast $\delta_C \simeq 1.686$ is the density contrast for a linear overdensity able to collapse at redshift z. Here ρ_M is the mean matter density at redshift z. For Gaussian fluctuations $\nu f(\nu) \propto \exp[-\nu^2/2]$ (Press & Schechter 1974), where the normalization constant is fixed by the requirement that all of the mass lies in a given halo $\int \nu f(\nu) d\nu = 1/2$ (White 2002). The evolution of the halo mass function $n(M, z)$ is mostly determined by the z dependence of $\sigma(R, z)$.

The rms amplitude of density fluctuations $\sigma^2(R, z)$ is related to the linear matter power spectrum $P(k,z)$ through (Jenkins et al. 2001)

$$\sigma^2(R, z) = \frac{D(z)^2}{2\pi^2} \int_0^{\infty} P(k, z)|W(kR)|^2 k^2 dk, \quad (6)$$

where $D(z)$ is the growth factor of linear perturbations normalized as $D(z = 0) = 1$ today, $W(kR)$ is the Fourier transform of the top-hat window function, and $W(x) = 3(\sin x - x \cos x)/x^3$. In Figure 3, we illustrate the $\sigma(M, z = 0)$ function for the different values of the effective magnetic field, $B_{\rm eff}$, and the spectral index n_B. The smaller amplitude of the magnetic field results in modifications at smaller mass scales. The $\sigma(M)$ dependence on the magnetic field characteristics is also derived in Kahniashvili et al. (2010), but, contrary to the case presented here, reflects *only* the $\sigma(M)$ induced by the pure magnetic field. In the present work we derive the effect of the magnetic field on the overall matter dispersion, including the standard density perturbations. The value of $\sigma(M)$ at $M = 2 \times 10^{14}\, M_{\rm Sun}$ is around 0.8 agreeing well with observational data (see Burenin & Vikhlinin 2012).

Numerical computation results for $n(M, z)$ are not accurately fit by the PS expression $\nu f(\nu) \propto \exp[-\nu^2/2]$ (see Sheth & Tormen 1999; Jenkins et al. 2001; Hu & Kravtsov 2003). Several more accurate modifications of $n(M, z)$ have been proposed. Here, we use the ST modification (Sheth & Tormen 1999) defined as (see Equation (5) of White 2002)

$$f(\nu) \propto [1 + (a\nu^2)^{-p}](a\nu^2)^{-1/2} \exp[-a\nu^2/2], \quad (7)$$

where the parameters $a = 0.707$ and $p = 0.303$ are fixed by fitting to the numerical results (for the PS case: $a = 1$ and $p = 0$; White 2001; Sheth & Tormen 1999). With this choice of parameter values, the mass of collapsed objects in Equation (7) must be defined using a fixed overdensity contrast with respect to the background density ρ_M, and this requires accounting for the mass conversion between M_{180b} and M_{200c}. Such a conversion depends on cosmological parameters (see Figure 1 of White 2001). Here, we use an analytical extrapolation of this figure to do the conversion for $\Omega_M \in (0.2, 0.35)$.

The difference induced by the magnetic field in the matter power spectrum $P(k)$ can potentially modify the δ_C parameter entering in Equation (7), which will result in different halo number counts. On the other hand, here we focus on the first-order effects, so we neglect all changes induced by the magnetic field in the Sheth–Tormen model parameter fitting (see Sheth & Tormen 1999). We also use the halo number count function at $z = 0$ because we are focusing only on the linear

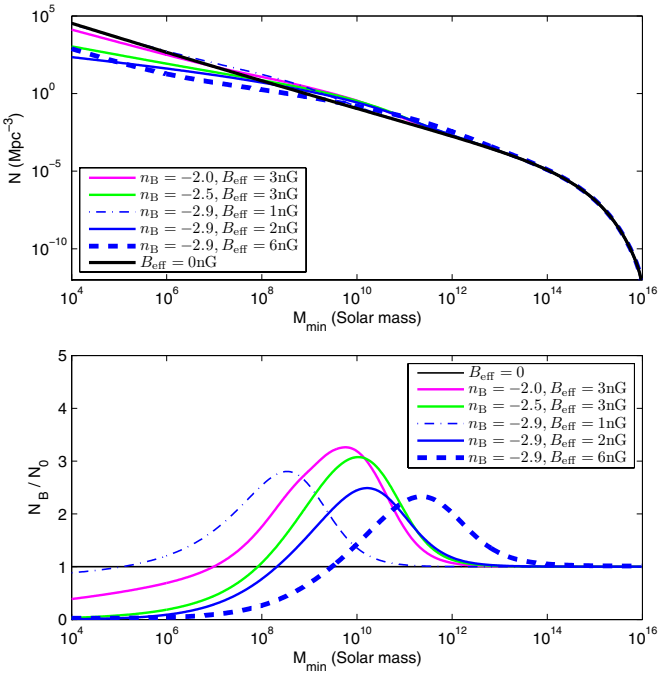

Figure 4. Halo number density $N(M > M_0)$ (top panel) and ratio of number density for magnetic and non-magnetic simulations $N_B)/N_0$ (bottom panel) for different effective magnetic field values $B_{\rm eff}$ and spectral index n_B, and $z = 0$. The number of small mass objects ($M \sim 10^4\, M_\odot$) in a magnetized case can be reduced down by a factor of 100 compared to the non-magnetic number; object number count excess occurs for objects with masses around $M \sim 10^{10}\, M_\odot$.

(A color version of this figure is available in the online journal.)

power spectrum, and all effects related to the magnetic field nonlinear evolution (see Schleicher & Miniati 2011) during the structure formation are neglected. We will present a more realistic scenario of the first object formation in future work.

In Figure 4 (top panel), we illustrate the halo mass function today ($z = 0$) for different values of $B_{\rm eff}$ and n_B. As we can see, the magnetic field presence affects the small mass ranges, reducing the abundance of low-mass objects. We do not present here any statistics using halo data accounting for several uncertainties involving cluster physics (Battaglia et al. 2012). On the other hand, we underline that the presence of a high enough magnetic field might be a possible explanation of the low-mass object abundance, which is one of the unsolved puzzles in ΛCDM cosmologies.

To get a better understanding of the magnetic field influence on the halo abundance, we plot the ratio of halo number density of ΛCDM models with and without magnetic fields (see Figure 4, bottom panel). In the high-mass limit, all magnetized ΛCDM models compared to the ΛCDM model predict slightly (a relative difference of the order of 10^{-5}) higher halo number density. Number density excess peaks around halos with masses $M \sim 10^{10}\, M_\odot$ and is strongly affected by the effective magnetic field value, as well as on the spectral shape. In contrast, at a low-mass limit $M < 10^7\, M_\odot$, the number of objects can be significantly lower than its non-magnetic value.

3.3. Lyα Data

The small-scale modifications induced by the primordial magnetic field must be reflected in first object formation in the universe, i.e., the objects at high redshifts. The most important class of such objects is damped Lyα absorption

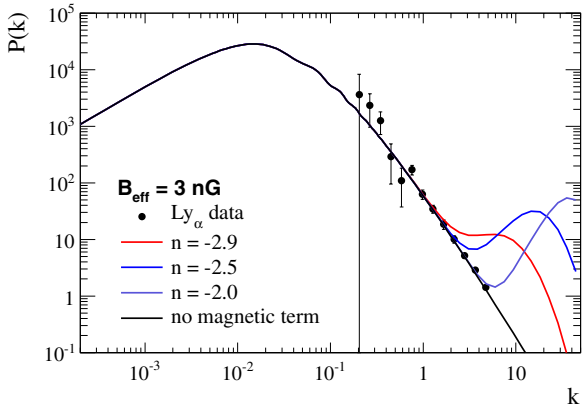

Figure 5. Magnetic field matter power spectra for different values of n_B and data points from Croft et al. (2002).

(A color version of this figure is available in the online journal.)

systems.[11] To describe these systems, it is possible to use semi-analytical modeling. Lyα systems have been used to constrain different cosmological scenarios (see McDonald et al. 2004 and references therein). Lyα data are very sensitive to the matter power spectrum around $k \simeq 10^{-1}$–10^2 Mpc^{-1}, wavenumbers that are affected by the primordial magnetic field (Shaw & Lewis 2012). As we will see below, these systems can be used to place stringent constraints on magnetic field properties.

We do not go through the detailed modeling of Lyα systems, leaving this for more precise computations, but we use the direct comparison of the reconstructed matter power spectrum and the theoretical matter power spectra affected by the primordial magnetic field.

For this study, we use Lyα data obtained by the Keck telescope (Croft et al. 2002). To get a conversion of data points (accounting that we use the wavevector k units h Mpc^{-1}), we multiply data by the conversion factor

$$\frac{100\,\sqrt{\Omega_m\,(1+z)^3+\Omega_\Lambda}}{1+z}$$

given in Kim et al. (1996). As the data is given at redshift 2.72, we translate the data to redshift zero by multiplying it by the square of the ratio of the growth factor at redshift zero to that at redshift 2.72. We compute the growth factors using the ICOSMOS calculator.[12] Thus, we multiply the data by 8.145 to estimate the Lyα data at redshift $z = 0$. The comparison of the theoretically predicted matter power spectrum and Lyα data is given in Figure 5.

We use χ^2 statistics to compare the predicted model with Lyα data. We assume no correlation between the uncertainties in the $P(\mathbf{k})$ measurements for different $\mathbf{k}$ values and find no evidence for primordial magnetic fields.

The 95% and 68% confidence level limits are given in Figure 6. The limits on B_λ are given Figure 7. We explicitly present the limits for $B_{\rm eff}$ and B_λ just to show that they have different behaviors when the spectral index is increasing.

[11] These objects have a high column density of neutral hydrogen ($N_{\rm H\,I} > 10^{20}$ cm^{-2}) and are detected by means of absorption lines in quasar spectra (Wolfe 1993). Observations at high redshift have lead to estimates of the abundance of neutral hydrogen in damped Lyα systems (Lanzetta et al. 1995). The standard view is that damped Lyα systems are a population of protogalactic disks (Wolfe 1993), with a minimum mass of $M = 10^{10}\, h^{-1}\, M_{\rm Sun}$ (Haehnelt 1995).

[12] ICOSMOS calculator is available at http://www.icosmos.co.uk/index.html.

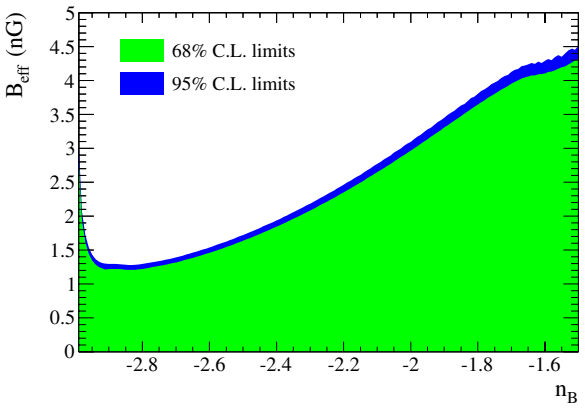

Figure 6. Effective magnetic field limits from Lyα data for different values of n_B.
(A color version of this figure is available in the online journal.)

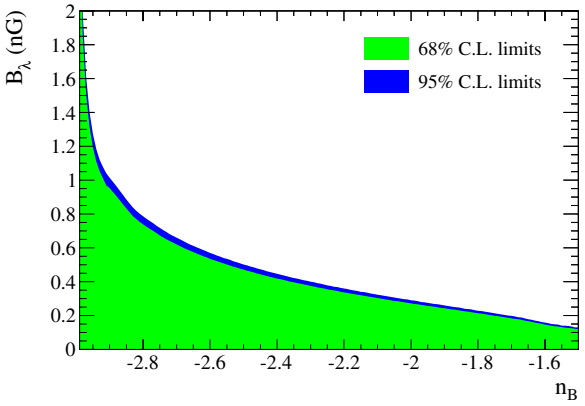

Figure 7. Smoothed magnetic field limits from Lyα for different values of n_B.
(A color version of this figure is available in the online journal.)

In terms of the total energy density of the magnetic field the limits are weaker if we are considering the redder spectra. At this point, the total energy density of the phase transition generated magnetic field is almost unconstrained.

3.4. The CMB Faraday Rotation Effect

As we have already noted above, the primordial magnetic field induces CMB polarization Faraday rotation, and for a homogeneous magnetic field the rotation angle is given by (Kosowsky & Loeb 1996)

$$\alpha \simeq 1.^\circ 6 \left(\frac{B_0}{1\,\mathrm{nG}}\right)\left(\frac{30\,\mathrm{GHz}}{\nu_0}\right)^2, \quad (8)$$

where B_0 is the amplitude of the magnetic field and ν_0 is the frequency of the CMB photons. In the case of a stochastic magnetic field, we have to determine the rms value of the rotation angle, $\alpha_{\rm rms}$, and the corresponding expression in terms of the effective magnetic field is given in Kahniashvili et al. (2010), being

$$\alpha_{\rm rms} \simeq 0.^\circ 14 \left(\frac{B_{\rm eff}}{1\,\mathrm{nG}}\right)\left(\frac{100\,\mathrm{GHz}}{\nu_0}\right)^2 \frac{\sqrt{n_B+3}}{(k_D\eta_0)^{(n_B+3)/2}} \times \left[\sum_{l=0}^{\infty}(2l+1)l(l+1)\int_0^{x_S} dx\, x^{n_B} j_l^2(x)\right]^{1/2}. \quad (9)$$

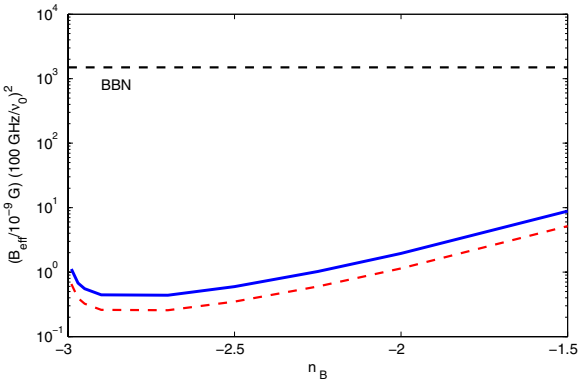

Figure 8. Effective magnetic field values for different spectral index n_B. The solid and dashed lines correspond to the 95% and 68% confidence levels, respectively. The upper limit set by BBN $B_{\rm eff} \sim \mu$G (Yamazaki & Kusakabe 2012; Kawasaki & Kusakabe 2012) is shown by the horizontal black line (BBN).
(A color version of this figure is available in the online journal.)

Here η_0 is the present value of conformal time, $j_l(x)$ is a Bessel function with argument $x = k\eta_0$, and $x_S = k_S\eta_0$ where $k_S = 2\,\mathrm{Mpc}^{-1}$ is the Silk damping scale. In the case of an extreme magnetic field which just satisfies the BBN bound, k_D might become less than the Silk damping scale. In this case, the upper limit in the integral above must be replaced by $x_D = k_D\eta_0$. Note that for $n_B \to -3$, Equation (9) is reduced to Equation (8) (see Kahniashvili et al. 2010 for details).

Here, we quote Komatsu et al. (2010) in order to determine the upper limits for the rms rotation angle. Adding the statistical and systematic errors in quadrature and averaging over *Wilkinson Microwave Anisotropy Probe* (*WMAP*; Komatsu et al. 2010), QUaD (Ade et al. 2008), and BICEP (Chiang et al. 2010; see Komatsu et al. 2010 for more details) with inverse variance weighting, the limits obtained were $\alpha = -0.^\circ 25 \pm 0.^\circ 58$ at (68% CL) or $-1.^\circ 41 < \alpha < 0.^\circ 91$ (95% CL). We obtain the rms values (absolute) of the rotation angle $|\alpha_{\rm rms}| < 0.^\circ 477$ and $|\alpha_{\rm rms}| < 0.^\circ 997$ (68% CL and 95% CL, respectively) assuming Gaussian statistics. In Figure 8, we display the upper limits of the effective magnetic field using the rotation angle constraints quoted above. Note that these limits are an order of magnitude better than obtained previously in Kahniashvili et al. (2010) where we used the *WMAP* 7 yr data alone. For an almost scale-invariant magnetic field, the limits are around 0.5 nG. As we can see for $n_B > -0.5$, the BBN limits on the effective magnetic field strength are stronger than those coming from the CMB faraday rotation effect. The situation is completely different when determining the limits for the smoothed magnetic field $B_{\lambda=1\,\mathrm{Mpc}}$ with $n_B > -2$, which are extremely strong from BBN (Caprini & Durrer 2001; Kahniashvili et al. 2011) and moderate in the case of the large-scale structures or the CMB birefringence; see above.

4. CONCLUSION

In this paper, we studied the large-scale signatures of cosmological magnetic fields generated during the radiation-dominated epoch prior to the BBN. We address such effects as the thermal tSZ effect, halo number density, and Lyα data. Due to several uncertainties present in tSZ and halo abundance tests, we find that Lyα measurements provide the tightest constraints on the primordial magnetic field energy density. We express these limits in terms of the effective value of the magnetic field, $B_{\rm eff}$. In the case of the scale-invariant spectrum $n_B = -3$, these

limits are identical to limits on the smoothed magnetic field B_λ (smoothed over a length scale λ that is conventionally taken to be 1 Mpc). For a steep magnetic field with spectral index $n_B = 2$, the difference between the limits derived in terms of the effective and smoothed field is several orders of magnitude. Also, limits have different behavior with increasing n_B. At this point, as we underlined previously (Kahniashvili et al. 2010), using the smoothed magnetic field can result in some confusion: the smoothed magnetic field at 1 Mpc scales is extremely small, while the total energy density of the magnetic field is maximal allowed by BBN bounds (see Yamazaki & Kusakabe 2012; Kawasaki & Kusakabe 2012 for more details on BBN bounds). The small values of the magnetic fields for $n_B = 2$ (that corresponds to the phase transition generated magnetic fields) might be treated as non-relevance on these fields. For example, in Shaw & Lewis (2012) it is claimed that the magnetic field with the spectral index greater than -2.5 is excluded (Shaw & Lewis 2012), while as shown in Kahniashvili et al. (2011) the magnetic field with extremely small smoothed field value B_λ at $\lambda = 1$ Mpc of the order of 10^{-29} G with the spectral index $n_B = 2$ can leave observable traces on the CMB and large-scale structure formation. The limits range between 1.5 nG and 4.5 nG for $n_B \in (-3; -1.5)$. These limits are comparable to those from the CMB polarization plane rotation. Our results can be applied with some precautions to the primordial magnetic fields generated in the matter-dominated epoch too; see Section 2.

Note when this paper was in the final stage of preparation, Pandey & Sethi (2013) showed that magnetic fields can be strongly constrained by first object formation, in particular through Lyα data.

We acknowledge useful comments from the anonymous referee. We thank R. Shaw for useful comments and discussion. The computation of the magnetic field power spectrum has been performed using the modified version of CAMB; for details, see Shaw & Lewis (2012). We appreciate useful discussions with A. Brandenburg, L. Campanelli, R. Croft, R. Durrer, A. Kosowsky, A. Kravtsov, F. Miniati, K. Pandey, B. Ratra, U. Seljak, S. Sethi, and R. Sheth. We acknowledge partial support from Swiss National Science Foundation SCOPES grant 128040, NSF grant AST-1109180, and NASA Astrophysics Theory Program grant NNXlOAC85G. T.K. acknowledges the ICTP associate membership program. A.N. and N.B. are supported by a McWilliams Center for Cosmology Postdoctoral Fellowship made possible by Bruce and Astrid McWilliams Center for Cosmology. A.T. acknowledges the hospitality of the McWilliams Center for Cosmology.

REFERENCES

Ade, P., Bock, J., Bowden, M., et al. (QUaD Collaboration) 2008, ApJ, 674, 22
Arlen, T. C., Vassiliev, V. V., Weisgarber, T., Wakely, S. P., & Shafi, S. V. 2012, arXiv:1210.2802
Arnaud, M., Pratt, G. W., Piffaretti, R., et al. 2010, A&A, 517, A92
Banerjee, R., & Jedamzik, K. 2003, PhRvL, 91, 251301
Battaglia, N., Bond, J. R., Pfrommer, C., & Sievers, J. L. 2012, ApJ, 758, 75
Battaglia, N., Bond, J. R., Pfrommer, C., Sievers, J. L., & Sijacki, D. 2010, ApJ, 725, 91
Beck, R., Brandenburg, A., Moss, D., Shukurov, A., & Sokoloff, D. 1996, ARA&A, 34, 155
Biskamp, D. 2003, Magnetohydrodynamic Turbulence (Cambridge: Cambridge Univ. Press)
Blasi, P., Burles, S., & Olinto, A. V. 1999, ApJL, 514, L79
Broderick, A. E., Chang, P., & Pfrommer, C. 2012, ApJ, 752, 22
Burenin, R. A., & Vikhlinin, A. A. 2012, AstL, 38, 347
Caprini, C., & Durrer, R. 2001, PhRvD, 65, 023517
Chiang, H. C., Ade, P. A. R., Barkats, D., et al. 2010, ApJ, 711, 1123
Croft, R. A. C., Weinberg, D. H., Bolte, M., et al. 2002, A&A, 581, 20
Dermer, C. D., Cavaldini, M., Razzaque, S., et al. 2011, ApJL, 733, L21
Dolag, K., Bartelmann, M., & Lesch, H. 2002, A&A, 387, 383
Dolag, K., Kachelriess, M., Ostapchenko, S., & Tomas, R. 2011, ApJL, 727, L4
Dunkley, J., Hlozek, R., Sievers, J., et al. 2011, ApJ, 739, 52
Durrer, R., & Caprini, C. 2003, JCAP, 11, 010
Essey, W., Ando, A. A., & Kusenko, A. 2012, APh, 35, 135
Fang, T., Humphrey, P. J., & Buote, D. A. 2009, ApJ, 691, 1648
Fedeli, C., & Moscardini, L. 2012, JCAP, 11, 055
Gopal, R., & Sethi, S. K. 2005, PhRvD, 72, 103003
Haehnelt, M. G. 1995, MNRAS, 273, 249
Hu, W., & Kravtsov, A. 2003, ApJ, 584, 702
Jedamzik, K., Katalinic, V., & Olinto, A. V. 1998, PhRvD, 57, 3264
Jenkins, A., Frenk, C. S., White, S. D. M., et al. 2001, MNRAS, 321, 372
Kahniashvili, T., Tevzadze, A. G., & Ratra, B. 2011, ApJ, 726, 78
Kahniashvili, T., Tevzadze, A. G., Sethi, S., Pandey, K., & Ratra, B. 2010, PhRvD, 82, 083005
Kandus, A., Kunze, K. E., & Tsagas, C. G. 2011, PhR, 505, 1
Kawasaki, M., & Kusakabe, M. 2012, PhRvD, 86, 063003
Kim, E., Olinto, A. V., & Rosner, R. 1996, ApJ, 468, 28
Kim, T. S., Viel, M., Haehnelt, M. G., Carswell, R. F., & Cristiani, S. 2004, MNRAS, 347, 355
Komatsu, E., & Seljak, U. 2002, MNRAS, 336, 1256
Komatsu, E., Smith, K. M., Dunkley, J., et al. (WMAP Collaboration) 2011, ApJS, 192, 18
Kosowsky, A., & Loeb, A. 1996, ApJ, 469, 1
Kravtsov, A., & Borgani, S. 2012, ARA&A, 50, 353
Kronberg, P. P., Bernet, M. L., Miniati, F., et al. 2008, ApJ, 676, 70
Kulsrud, R. M., & Zweibel, E. G. 2008, RPPh, 71, 0046091
Lanzetta, K. M., Wolfe, A. M., & Turnshek, D. A. 1995, ApJ, 440, 435
Lueker, M., Reichardt, C. L., Schaffer, K. K., et al. 2010, ApJ, 719, 1045
Mack, A., Kahniashvili, T., & Kosowsky, A. 2002, PhRvD, 65, 123004
McDonald, P., Seljak, U., Cen, R., et al. 2005, ApJ, 635, 761
Neronov, A., & Vovk, I. 2010, Sci, 328, 73
Pandey, K. L., & Sethi, S. K. 2013, ApJ, 762, 15
Paoletti, D., & Finelli, F. 2012, arXiv:1208.2625
Press, W. H., & Schechter, P. 1974, ApJ, 187, 425
Reichardt, C. L., Shaw, L., Zahn, O., et al. 2012, ApJ, 755, 70
Schleicher, D. R. G., & Miniati, F. 2011, MNRAS, 418, L143
Shaw, J. R., & Lewis, A. 2012, PhRvD, 86, 043510
Shaw, L. D., Nagai, D., Bhattacharya, S., & Lau, E. T. 2010, ApJ, 725, 1452
Sheth, R. K., & Tormen, G. 1999, MNRAS, 308, 119
Springel, V. 2010, ARA&A, 48, 391
Subramanian, K., & Barrow, J. D. 1998, PhRvD, 58, 083502
Subramanian, K., Shukurov, A., & Haugen, N. E. L. 2006, MNRAS, 366, 1437
Tashiro, H., & Sugiyama, N. 2011, MNRAS, 411, 1284
Tashiro, H., Takahashi, K., & Ichiki, K. 2012, MNRAS, 424, 927
Tavecchio, F., Ghisellini, G., Foschini, L., et al. 2010, MNRAS, 406, L70
Trac, H., Bode, P., & Ostriker, J. P. 2011, ApJ, 727, 94
Vallée, J. P. 2004, NewAR, 48, 763
Vazza, F., Tormen, G., Cassano, F., Brunetti, G., & Dolag, K. 2006, MNRAS Lett., 369, L14
White, M. 2001, A&A, 367, 27
White, M. 2002, ApJS, 143, 241
Widrow, L. M. 2002, RvMP, 74, 775
Wolfe, A. 1993, in Relativistic Astrophysics and Particle Cosmology, ed. C. W. Ackerlof & M. A. Srednicki (New York: New York Academy of Science), 281
Yamazaki, D. G., Ichiki, K., Kajino, T., & Mathews, G. J. 2012, AdAst, 2010, 586590
Yamazaki, D. G., & Kusakabe, M. 2012, PhRvD, 86, 123006